# GAUSSIAN3DIFF: 3D Gaussian Diffusion for 3D Full Head Synthesis and Editing

Yushi Lan[1,2*]    Feitong Tan[1]    Di Qiu[1]    Qiangeng Xu[1]    Kyle Genova[1]    Zeng Huang[1]
Sean Fanello[1]    Rohit Pandey[1]    Thomas Funkhouser[1]    Chen Change Loy[2]    Yinda Zhang[1]
[1] Google        [2] S-Lab, Nanyang Technological University, Singapore

Figure 1. GAUSSIAN3DIFF adopts 3D Gaussians defined in UV space as the underlying 3D representation, which intrinsically support high-quality novel view synthesis, 3DMM-based animation and 3D diffusion for unconditional generation.

## Abstract

*We present a novel framework for generating photorealistic 3D human head and subsequently manipulating and reposing them with remarkable flexibility. The proposed approach leverages an implicit function representation of 3D human heads, employing 3D Gaussians anchored on a parametric face model. To enhance representational capabilities and encode spatial information, we embed a lightweight tri-plane payload within each Gaussian rather than directly storing color and opacity. Additionally, we parameterize the Gaussians in a 2D UV space via a 3DMM, enabling effective utilization of the diffusion model for 3D head avatar generation. Our method facilitates the creation of diverse and realistic 3D human heads with fine-grained editing over facial features and expressions. Extensive experiments demonstrate the effectiveness of our method. Please check our website.*

## 1. Introduction

Generating and editing photorealistic portraits is one of the cruxes of computer vision and graphics and has tremendous demand in downstream applications, such as embodied AI, VR/AR, digital games, and the movie industry. Emerging neural radiance field, 3D-aware GANs [1, 8, 9, 21, 59] have

achieved great success in generating high-quality multi-view consistent portrait images with volumetric rendering. Editing capabilities for 3D-aware GANs have also been achieved through latent space auto-decoding, altering a 2D semantic segmentation [62, 63], or modifying the underlying geometry scaffold [64]. However, generation and editing quality tends to be unstable and less diversified due to the inherent limitation of GANs, and detailed-level editing is not well supported due to feature entanglement in the compact latent space or tri-plane representations.

Recently, diffusion models [24, 61] have been proposed for high-quality content generation, achieving competitive performance compared to traditional GAN-based approaches [14]. Efforts have been made on 3D-aware portrait generation by de-noising on the tri-plane representation [60, 66], which, however, do not support expression and region-based editing.

In this paper, we present GAUSSIAN3DIFF, a diffusion-based generative model designed for 3D volumetric heads. This model enables unconditional generation while offering versatile capabilities for both flexible global and fine-grained region-based editing, such as change of face shape, expression, or appearance. As the core of our model, we propose a novel representation of the 3D head, in which complex volumetric geometry and appearance are encoded by a large set of 3D Gaussians modulated by tri-planes anchored on the surface of an underlying 3D face parametric model (3DMM). We further formulate such a 3DMM surface attached representation into the UV space of the

1

3DMM, where each texel stores a flattened vector including 3D Gaussian parameters and the tri-plane embeddings. We find that this representation excels, especially in geometry and expression-based editing, due to its rich semantic connection with the 3DMM model. Furthermore, it facilitates smooth interpolation and exchange of local or global textures, due to the dense correspondence established in the UV space. Lastly, its 2D UV formatting ensures immediate compatibility with the well-established learning framework of 2D diffusion models [58].

To this end, we propose a novel analysis-by-synthesis approach to learn a diffusion model, in which we simultaneously reconstruct large amounts of 3D heads in our representation by learning a shared latent space via an auto-decoder [48] with multi-view supervision. Compared to per-example fitting, we empirically find that the jointly optimized shared latent space encourages the alignment of local 3D Gaussians, which in turn benefits diffusion learning. We demonstrate the effectiveness of our framework by following a DatasetGAN [75] paradigm, where the experiments are conducted on samples generated from a 3D-aware GAN, *i.e.*, Panohead [1], which ensures us good enough fidelity and diversity. Trained on piles of *single-expression* identities only, GAUSSIAN3DIFF achieves high-quality 3D reconstruction with the intrinsic support for 3DMM-drivable editing, and compares favorably to existing volumetric avatar generation approaches. Furthermore, we showcase the superior editing ability of our framework with inter-subject attribute transfer, and various fine-grained editing tasks such as local region-based editing and 3D in-painting with appealing visual quality.

Our contributions are summarized as follows. We propose a novel representation for 3D volumetric head - 3D Gaussian modulated local tri-plane on 3DMM UV space, which naively supports flexible editing capability. We propose a novel auto-decoding-based fitting algorithm to generate training data in our representation and show it benefits diffusion model training. Extensive experiments demonstrate that our method exhibits superior data generation quality and editing capability.

## 2. Related Work

**3D-aware GAN.** Generative Adversarial Networks [19] have shown promising results in generating photorealistic images [6, 29, 30] and inspired researchers to investigate using them for 3D aware generation [23, 42, 45]. Motivated by the recent success of neural rendering [39, 40, 48], researchers extend NeRF [40] to generation [8, 25, 59] and achieve impressive 3D-awareness synthesis. To increase the generation resolution, recent works [1, 9, 21, 43, 44, 65] resorted a hybrid design to high resolution up to 512. However, samples from these methods cannot easily be edited. On the other hand, FENeRF [62] and IDE-3D [63] proposed

to generate, edit and animate human faces, guided by a segmentation map. However, their support for local editing is still unsatisfactory, as the local geometry cannot be explicitly edited due to the lack of spatial information in the segmentation map. Additionally. Moreover, segmentation-driven animation has several limitations, *e.g.*, can only animate an identity with similar foreface layout. By contrast, GAUSSIAN3DIFF achieves improved performance and flexibility via direct basic-model-driven animation.

Another line of work [4, 26, 27, 33, 34, 46, 68, 75] propose to use a pre-trained GAN to generate training data. Through careful design in the sampling strategy [27], loss functions [46] and generation process [75], off-the-shelf generators can facilitate a series of downstream applications. In this work, we also adopt a pre-trained 3D GAN as an "infinite" source of 3D assets.

**Diffusion Model.** Despite the remarkable success of GANs, diffusion-based models [14, 24, 61] have recently shown impressive performance over various generation tasks, especially for 2D tasks like text-to-image synthesis [55, 57]. However, applying diffusion to 3D generation is still under-explored. Pioneering attempts have been made on shape [10, 41], point cloud [70], and text-to-3D [15, 28, 52] generation. Recently, some works have succeeded in training diffusion models from 2D images for unconditional 3D generation [2, 22] of human faces and objects. However, the global 3D tri-plane in these approaches makes it difficult to edit and animate the resulting 3D representation, limiting their use for avatars.

## 3. Method

We propose GAUSSIAN3DIFF, a comprehensive framework designed for the generation of photo-realistic 3D human heads with extensive editing capabilities. To fulfill this objective, we introduce a novel 3D head avatar representation in Sec. 3.1. This representation leverages 3D Gaussians with local tri-planes and effectively encodes geometric and textural information in local regions. Critically, the 3D Gaussians are anchored to a 3D Morphable Model (3DMM), allowing for the parameterization of 3D volumetric data into the 2D texture space. This facilitates the application of a 2D diffusion model for the editing process. In Sec. 3.2, we illustrate the diffusion-based avatar editing framework. Initially, we delineate our analysis-by-synthesis approach that concurrently reconstructs a large number of avatars of *different expressions* and learns a shared latent space through multi-view supervision. This ensures the learned representations of all avatars encapsulate crucial mutual information. Subsequently, we account for the training of a 2D diffusion model that generates avatars with *neutral expression*. In Sec. 3.3, we discuss the editing mechanisms to showcase the capabilities of the proposed method.

$9+3\times S_x\times S_y\times C$

Gaussians in 3D

$g_1 = 0.3$

$\phi$ → $c$
→ $\alpha$

RBF
Blending

VR

SR

$g_2 = 0.5$

$H$

$g_3 = 0.2$

$W$

Gaussians
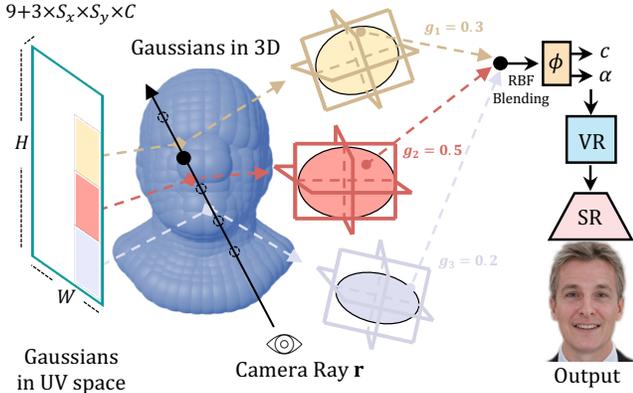in UV space

Camera Ray **r**

Output

Figure 2. During volume rendering, tri-plane payloads in UV space are projected onto 3D space with Gaussian pose parameters. For each shading point, we query the texture and geometry information from the three nearest Gaussian payloads, with influence strength defined using a radial basis function (RBF). The low-res 2D rendering is then upsampled with a CNN-based super-resolution network.

## 3.1. Avatar Representation

**3D Gaussian with tri-plane payload.** Existing methods represent a 3D head with a global representation [17, 20, 49, 63, 66, 76], where either a single MLP [17, 20, 49, 76] or a tri-plane [63, 66] is employed to encode the entire neural radiance field. However, the global-based representation limits the region-based editing ability and cannot be directly driven by the parametric models [35, 38, 51]. Inspired by previous work [7, 36, 73] on representing radiance fields with local primitives, we propose to represent a 3D human head as a set of local tri-planes, each modulated by a 3D Gaussian initialized from a 3DMM. Specifically, each 3D Gaussian $\mathcal{G}_i = \{\boldsymbol{\mu}_i, \Sigma_i, P_i\}$ is characterized by 9 pose parameters and a payload - a 3D center $\boldsymbol{\mu}_i$, 3 axis-aligned radii and 3 rotation angles parameterized by a 6-DOF covariance matrix $\Sigma_i$, and a tri-plane payload $P_i \in \mathbb{R}^{3\times S_x \times S_y \times C}$. These pose parameters define the local coordinate transform from the world space to the tri-plane space, as well as the influence strength. Each point $\mathbf{x}$ in the world space can be mapped to the canonical local space according to the 3D Gaussian's center $\boldsymbol{\mu}$ and rotation following [31, 74]. The influence strength is defined as an analytic radial basis function (RBF):

$$g(\mathbf{x}) = \exp\left(-\frac{1}{2}\left(\mathbf{x}-\boldsymbol{\mu}\right)^T \Sigma^{-1}\left(\mathbf{x}-\boldsymbol{\mu}\right)\right). \quad (1)$$

Given a scene integrated by Gaussians, we can render any view with volumetric rendering [40]:

$$\hat{C}(\mathbf{r}) = \sum_{j=1}^{J} T_j \alpha_j \mathbf{c}_j, \text{where } T_j = \prod_{l=1}^{j-1}(1-\alpha_l). \quad (2)$$

where $\hat{C}(\mathbf{r})$ is the rendered color from the ray $\mathbf{r}$, $T_j$ is transmission at the $j$-th sample along the ray, $\alpha_j, \mathbf{c}_j$ are the opacity and color of the sample, and $J$ total number of samples along the ray. To efficiently compute $c_j, \alpha_j$ of each sample point $\mathbf{x}_j$, we only query $K$ nearest Gaussian payloads $\mathcal{G}_k$ measured by the Euclidean distance to the Gaussian centers $\boldsymbol{\mu}_k$. The queried features are transformed to the corresponding $\mathbb{R}^4$ values via a shared tiny rendering MLP $\phi$. We then take a weighted average of the $k$ individual color and opacity by:

$$\mathbf{c}_j = \sum_{k=1}^{K} \hat{g}_k(\mathbf{x}_j)\mathbf{c}_{j,k}, \quad (3)$$

$$\alpha_j = \sum_{k=1}^{K} g_k(\mathbf{x}_j)\alpha_{j,k}, \quad (4)$$

$$\text{where } \hat{g}_k(\mathbf{x}_j) = \frac{g_k(\mathbf{x}_j)}{\sum_{k=1}^{K} g_k(\mathbf{x}_k) + \epsilon}, \quad (5)$$

where $\mathbf{c}_{j,k}$ and $\alpha_{j,k}$ represent the color and opacity of point $\mathbf{x}_j$ queried from Gaussian $\mathcal{G}_k$. $\hat{g}_k(\mathbf{x}_j)$ denotes the normalized inference strength and $\epsilon$ serves as a factor allowing smooth decay. Note that we do not normalize $g_i(\mathbf{x}_k)$ when computing opacity $\alpha_j$. This choice allows the opacity $\alpha_j$ to naturally decay in empty space. This strategy acts as a window function [37], encouraging the Gaussians to focus on the local surface region.

In practice, we found a good balance between capacity and storage by using a total of $N = 1024$ Gaussians, each associated with a local tri-plane of spatial dimensions $S_x = S_y = 8$, and $C = 8$ for every feature plane within the local tri-plane. Our approach is thus more efficient than previous 3D Gaussian-based representations [31, 32] that require millions of tiny blobs where each only stores the spherical harmonic (SH) coefficients and opacity value.

**UV Space Representation.** By anchoring the 3D Gaussian payloads on a 3DMM, each payload now corresponds precisely to a specific 2D location on the texture map. Consequently, these Gaussians stored on the UV space can be processed with the U-Net-based diffusion framework [55]. Furthermore, the semantically aligned texture map facilitates a range of editing operations.

Specifically, following previous work on the dynamic avatar reconstruction [3, 36], we first register a 3DMM model, *e.g.*, FLAME [35] for each identity instance generated from pretrained 3D GAN. Vertices on fitted 3DMM model can be directly rasterized onto the UV space, where a 3D Gaussian is attached to each rasterized vertex.

We utilize the vertex positions to initialize $\boldsymbol{\mu}_i$, and face normals to initialize the rotations. The axis-aligned anisotropic scaling is initialized proportionally to the area of the corresponding faces on the mesh. Moreover, to maintain flexibility over out-of-model regions such as hair and
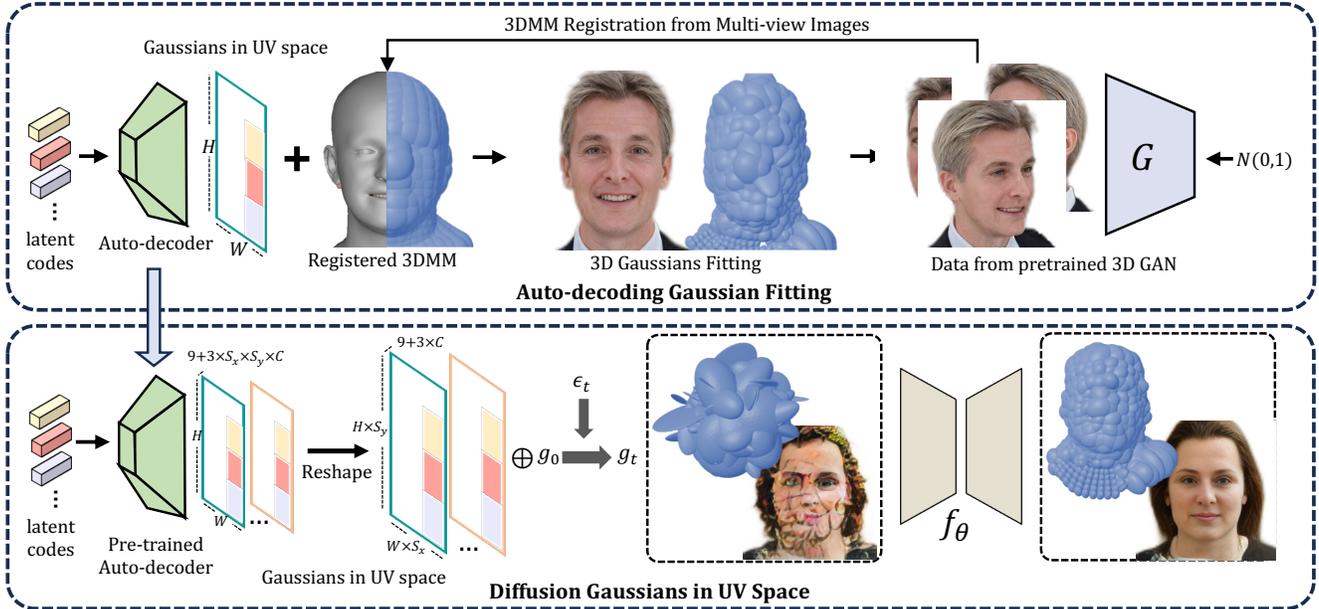
Figure 3. Pipeline of learning 3D head generation. Top: An autoencoder is trained to generate 3D Gaussians with payloads in UV space from a dataset produced by a pretrained 3D GAN; Bottom: a diffusion model is trained by a diffusion and denoising process on the 3D Gaussians, generated by the auto-decoder trained in the previous step.

glasses, all of the Gaussian parameters are allowed to be optimized during reconstruction.

The overall trainable parameters of each identity consist of the 9-DOF Gaussians over the UV grid: $\boldsymbol{\mu} \in \mathbb{R}^{H \times W \times 3}$, $\Sigma \in \mathbb{R}^{H \times W \times 6}$, and the corresponding local payloads: $P \in \mathbb{R}^{H \times W \times 3 \times 8 \times 8 \times 8}$.

## 3.2. Learning 3D Head Generation

**Reconstruction 3D Heads with an Auto-Decoder.** To effectively train the diffusion model, it is essential to have a large dataset of high-quality photorealistic 3D head assets. To address this issue, we employ the DatasetGAN [33, 34, 75] paradigm and utilize Panohead [1], a state-of-the-art 3D GAN for generating human heads, as our data generator. This approach enables us to prepare a sufficient number of 3D assets for 3D Gaussian fitting and diffusion training.

Fitting 3D assets individually involves costly reconstruction over dense multi-view images from scratch, making it data-intensive and inefficient. To overcome this challenge, we adopt an auto-decoding design [5, 47, 54] that learns a shared decoder to reconstruct 3D heads by optimizing a latent code from multi-view images. Specifically, each 3D instance is associated with a latent code $\mathbf{z} \in \mathbb{R}^{512}$ during the optimization process. This latent code can be decoded into the local payloads in UV space through a convolutional decoder $D : \mathbb{R}^{512} \to \mathbb{R}^{H \times W \times 3 \times S_x \times S_y \times C}$. Unlike previous work [66] that fits tri-plane independently, our shared decoder is trained from multiple instances, enabling faster convergence and improved generalizability. Furthermore,

decoding all local payloads from a shared decoder results in a smooth latent space suitable for diffusion training.

Similar to PanoHead [1], in order to reduce the memory consumption and computation cost, we render the color image in low resolution from 3D Ganssians and upsample them to high resolution with a super-resolution module.

During the training process, we jointly optimize all network parameters and the latent code. The loss function is decomposed into RGB loss, opacity regularization, and latent code regularization.

$$\mathcal{L} = \mathcal{L}_{\text{rgb}} + \mathcal{L}_{\text{reg}} + \mathcal{L}_{\text{code}}. \tag{6}$$

where $\mathcal{L}_{\text{rgb}}$ is the RGB loss measured with L1 and LPIPS [72] between the synthesized color $\hat{C}$ and the ground truth color $C$ within each patch, $\mathcal{L}_{\text{reg}}$ regularizes a compact 3D representations and $\mathcal{L}_{\text{code}}$ penalize the norm of the latent code given a normal prior [5].

**3D Gaussian Diffusion in the UV Space.** After the 3D Gaussians are prepared in UV space, we could learn a diffusion prior on the 3D Gaussians to support 3D avatar generation. Specifically, a diffusion model generates data by learning the reverse of a destruction process, which is commonly achieved by gradually adding Gaussian noise over time. It is convenient to express the process directly in the marginals $q(\mathcal{G}_t|\mathcal{G}_0)$ which is given by:

$$q(\mathcal{G}_t|\mathcal{G}_0) = \mathcal{N}(\mathcal{G}_t|\alpha_t \mathcal{G}_0, \sigma_t^2 \mathbf{I}) \tag{7}$$

where $\alpha_t, \sigma_t \in (0, 1)$ are hyperparameters that determine how much signal is destroyed at a timestep $t$. Commonly,

we consider variance preserving [61] process with $\alpha_t^2 = 1 - \sigma_t^2$. Before diffusion training, we drive $\mathcal{G}_0$ to *neutral expression*. This ensures the subsequent generated samples can be directly manipulated using the expression basis [35]. **Forward Process.** Assuming the diffusion process is Markov, the forward transition is given by:

$$q(\mathcal{G}_t|\mathcal{G}_s) = \mathcal{N}(\mathcal{G}_t|\alpha_{ts}\mathcal{G}_s, \sigma_{ts}^2\mathbf{I}), \qquad (8)$$

where $\alpha_{ts} = \alpha_t/\alpha_s$ and $\sigma_{ts}^2 = \sigma_t^2 - \alpha_{t|s}^2\sigma_s^2$ and $t > s$. To improve the performance of the diffusion model, which favors narrower input channels [55], we unfold local tri-planes onto UV space along the $x$ and $y$ dimensions. This operation reshapes the Gaussian representation on UV from $\mathbb{R}^{W \times W \times (9+3 \times S_x \times S_y \times C)}$ to $\mathbb{R}^{(W \times S_x) \times (W \times S_y) \times (9+3 \times C)}$, 9-d Gaussian parameters are replicated $S_x \times S_y$ times within each local tri-plane during the unfolding.

**Denoising Process.** Conditioned on a single datapoint $\mathcal{G}$, the denoising process can be written as:

$$q(\mathcal{G}_s|\mathcal{G}_t, \mathcal{G}_0) = \mathcal{N}(\mathcal{G}_t|\boldsymbol{\mu}_{t\to s}, \sigma_{t\to s}^2\mathbf{I}). \qquad (9)$$

where $\boldsymbol{\mu}_{t\to s} = \frac{\alpha_{ts}\sigma_s^2}{\sigma_t^2}\boldsymbol{z}_t + \frac{\alpha_s\sigma_{ts}^2}{\sigma_t^2}\boldsymbol{x}$ and $\sigma_{t\to s} = \frac{\sigma_{ts}^2\sigma_s^2}{\sigma_t^2}$. The literature shows [61] that by approximating $\mathcal{G}_0$ by a denoiser $\hat{\mathcal{G}}_0 = f_\theta(\mathcal{G}_t)$, we can define the learned distribution $p(\mathcal{G}_s|\mathcal{G}_t) = q(\mathcal{G}_s|\mathcal{G}_t, \boldsymbol{x} = \hat{\mathcal{G}}_0)$ without loss of generality as $s \to t$.

In practice, we train the denoiser $f_\theta$ to predict the input gaussian $\mathcal{G}_0$ such that:

$$\mathcal{L}_t^{\text{ddpm}} := \mathbb{E}_{\mathcal{G}, \epsilon \sim \mathcal{N}(0,1), t}\left[w_t\|\mathcal{G}_0 - f_\theta(\mathcal{G}_t, t)\|_2^2\right]. \qquad (10)$$

where the denoiser $f_\theta(\circ, t)$ of our model is realized as a time-conditional U-Net [56]. We choose an empirical $w_t = \text{S}(\text{SNR}(t))$ where $\text{SNR}(t) = \alpha_t^2/\sigma_t^2$ and S is the sigmoid function, as in [22].

### 3.3. Editing Mechanism

We emphasize three key advantages of our proposed method and explore their potential applications. **1)**: Local Gaussians with 3DMM template. In contrast to global-based 3D representations [1, 18, 22, 49, 50, 63] where each attribute is intricately entangled, our method gains advantage by integrating 3D scenes with local Gaussians. This approach allows for isolating and controlling local edits without unintended propagation to the global representation. Additionally, anchoring the Gaussians over 3DMM inherits the benefits of a 3DMM, enables direct identity and expression editing. **2)**: UV-space parameterization. By rasterizing the 3DMM onto semantically consistent UV space, our method facilitates flexible region-based editing Specifically, we can directly transfer [33] specific semantic regions, such as the mouth or nose, across identities by swapping their learned local Gaussians. Leveraging the trained

Table 1. **Quantitative performance.** GAUSSIAN3DIFF achieves competitive performance over 3D-related metrics (ID, Depth) and SoTA performance on the expression editing (PCK) performance. Additionally, yields faster rendering with less storage required with competitive 3D metrics.

| Methods | ID ↑ | Depth ↓ | PCK@2.5 ↑ | PCK@5 ↑ | FPS ↑ | Storage(MB) ↓ |
|---------|------|---------|-----------|---------|-------|----------------|
| FENeRF | 0.61 | 2.71 | - | - | 1.2 | 10 |
| Panohead | **0.80** | 2.32 | - | - | 19 | 72 |
| IDE-3D | 0.76 | **1.71** | 0.16 | 0.33 | 25.1 | 48 |
| Ours | 0.78 | 2.58 | **0.783** | **0.99** | **47/27** | **8.25** |

diffusion model, we can further edit the region by diffusing the masked region in UV space to while keeping the remaining areas frozen. **3)** Geometry-texture disentanglement. Empowered by floatable 3D Gaussians with tri-plane payload, a noteworthy byproduct benefits of GAUSSIAN3DIFF is the support of geometry-texture disentanglement. All the aforementioned editing applications can be conducted on either geometry, texture, or both.

## 4. Experiment

**Dataset.** To maintain both quality and diversity, we sample $10,000$ 3D portraits from pre-trained Panohead [1] with diverse identities and expressions. For each identity, we render 50 multi-view images and depths with known camera poses. We use the $64 \times 64$ view-consistent 3D renderings for Gaussian fitting, and the $512 \times 512$ samples for super-resolution training. We filter out the low-quality samples using CLIP [53].

**Implementation Details.** We use $N = 1024$ Gaussians to represent each 3D identity, given $H = W = 32$. During rendering, we adopt $K = 3$ for nearby Gaussian blending. The autodecoder $D$ is implemented similarly to Style-GAN [29] with noise injection removed. After the $D$ is trained, we further stack a $\times 4$ super-resolution model above it with the architecture from ESRGAN [67]. The denoiser $f_\theta$ is implemented as a 2D U-Net with architecture from Imagen [58]. The decoded UV maps of all instances are exported from the trained autodecoder $D$ as the training corpus of the diffusion model $f_\theta$. We use 2 A6000 GPUs for model training.

**Evaluation Metrics.** We select a series of proxy metrics to benchmark our method. Following [63], we evaluate view consistency assessed by multi-view facial identity consistency (ID) [13] rendered from random camera poses. To evaluate the synthesized 3D geometry, we follow EG3D [9] to use an off-the-shelf tool to estimate depth maps from renderings and compute L2 distance against rendered depths. Moreover, we adopt an avatar-centric metric, Percentage of Correct Keypoints (PCK) [69] to evaluate the expression editing ability. The rendering speed and storage are also included.
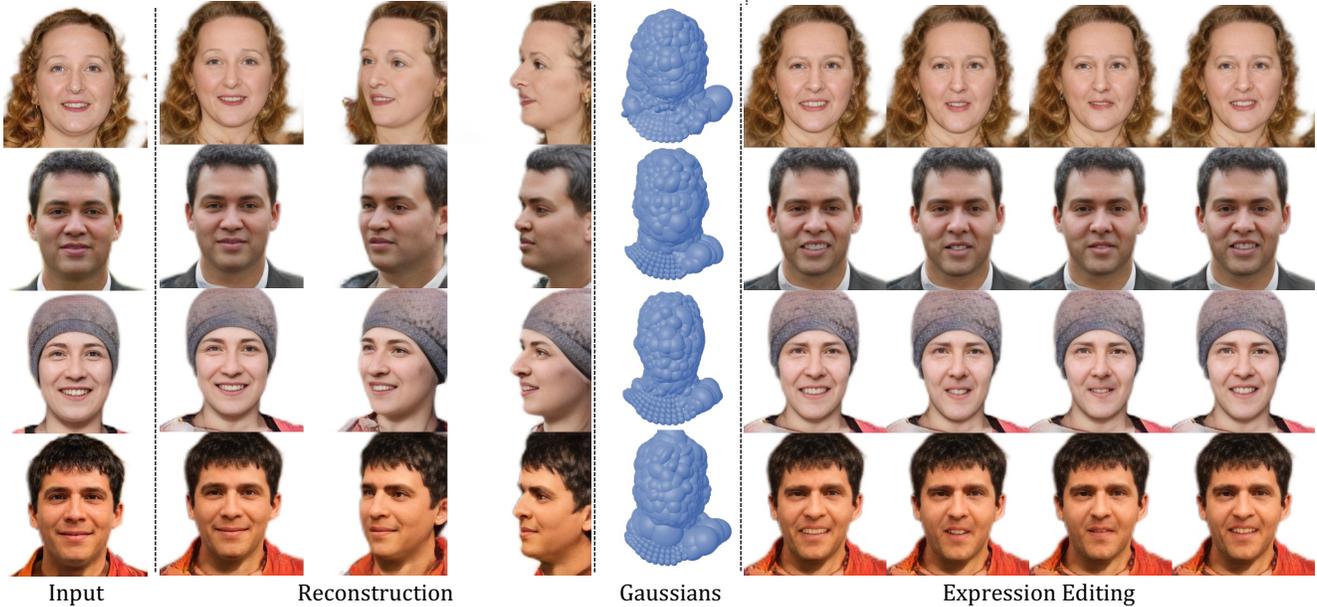
| Input | Reconstruction | Gaussians | Expression Editing |

Figure 4. **Auto-Decoder Results.** With the local Gaussians and tri-plane design, our auto-decoder $D$ yield high-quality and view-consistent reconstructions. Moreover, GAUSSIAN3DIFF intrinsically support novel expression animation by moving the positions of the optimized Gaussians. Note that we do not rely on multi-expression dataset during training.

## 4.1. Quantitative Comparisons

The results of numerical comparisons are presented in Tab. 1. Given that our method leverages Panohead data for training, it exhibits similar performance on ID and Depth metrics. In terms of expression editing ability, conventional global-based methods such as FeNeRF and Panohead do not support animation. Though IDE-3D supports segmentation-based reenactment, it lacks identity preservation and falls behind the PCK metric. GAUSSIAN3DIFF stands out as the only method that supports 3DMM-driven expression editing and achieving better PCK performance under both thresholds. Moreover, GAUSSIAN3DIFF supports faster rendering (47 FPS w/o SR and 27 FPS with SR) with less storage required for synthesized human heads.

## 4.2. Qualitative Evaluations

**Auto-decoded Gaussians.** We first visualize the Gaussians reconstruction from the autodecoder $D$ in columns $1-4$ of Fig. 4. The reconstruction produces high-fidelity and view-consistent view synthesis. Additionally, the corresponding optimized Gaussians align with the identity shape of the input, showcasing the robust capacity of our design.

**Expression Editing.** We further include the novel expression editing performance in columns $5-8$ Fig. 4. Despite being trained on collections of identities with a single expression, GAUSSIAN3DIFF inherently supports 3DMM-based expression editing by manipulating the underlying 3D Gaussians. Furthermore, owing to the autodecoder design, GAUSSIAN3DIFF can learn diverse expressions across iden-

tities, yielding natural-looking results under novel expressions.

**Shape-Texture Transfer.** GAUSSIAN3DIFF naturally supports geometry-texture disentanglement, where Gaussians managing the geometry and attached local tri-planes determining the texture within a local region defined on the UV map.

We present the interpolation trajectory of the shape-texture transfer in Fig. 5, where both shape and texture are gradually added from the source identity to the target. The semantically meaningful intermediate results in both shape and texture interpolation validate the effectiveness of our design.

**Unconditional Generation.** Thanks to the compact UV space design, we can directly leverage powerful 2D diffusion architectures for 3D-aware generation. Specifically, we train a diffusion model $\epsilon_\theta$ over the exported UV maps from the autodecoder $D$ and include the diffusion generation results in Fig. 6. Visually inspected, the diffusion-generated results maintain the same high-fidelity and view-consistent renderings as the reconstruction results with diverse sampling. Compared with the previous tri-plane-based method [1, 66], GAUSSIAN3DIFF maintains high capacity, and flexibility and intrinsically avoids Janus problem. Besides, diffusion models process better editing ability compared with GAN-based methods.
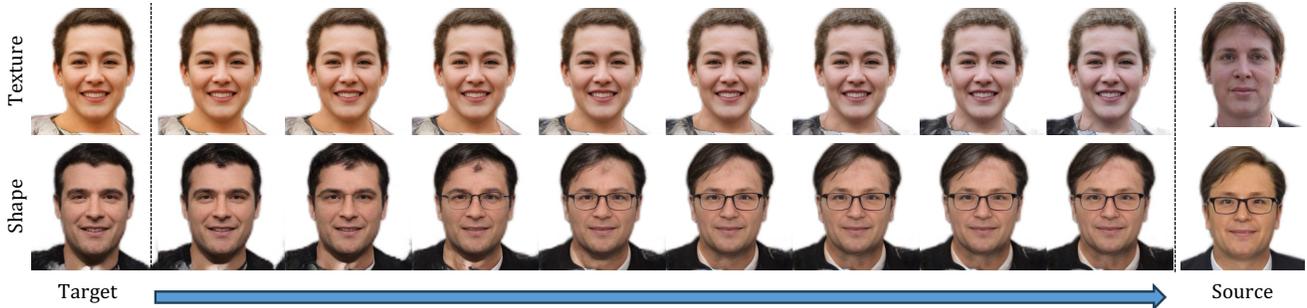
Figure 5. **Shape-Texture Interpolation.** We visualize the intermediate trajectory of texture transfer in row−1, and the shape transfer in row−2. Both shape and texture interpolation results preserve high-fidelity during the middle state.
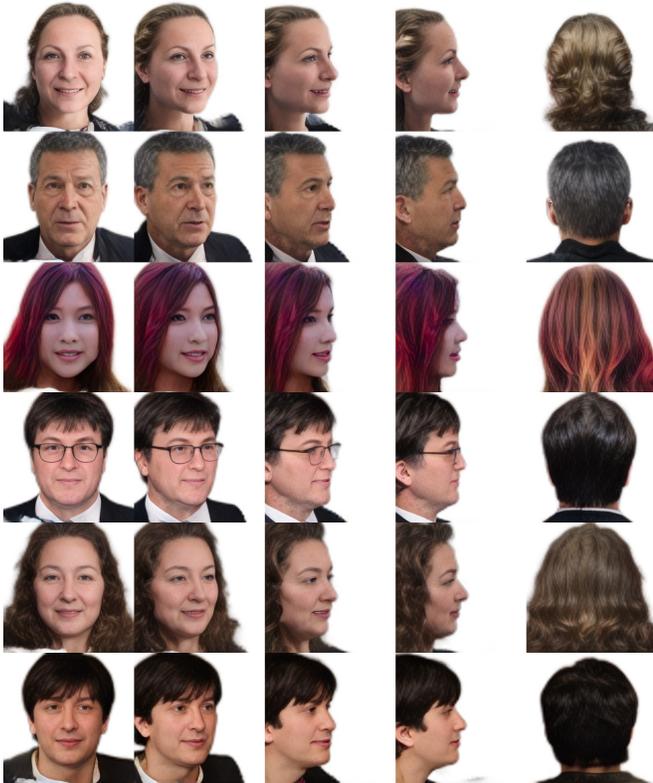


Figure 6. **Unconditional Diffusion Sampling.** The compact UV space design allows us to leverage 2D diffusion architectures for 3D aware synthesis.

## 4.3. Applications

**3D Inpainting using Diffusion Model.** First, we showcase both the geometry- and texture-based inpainting in Fig. 7, where unmask the *upper face in the UV space* and let the diffusion model inpaints the remaining areas. Both yield holistically reasonable results while keeping the corresponding inputs within the mask unchanged.

**3DMM-based Editing.** GAUSSIAN3DIFF marries the best of both the model-based 3DMM and neural representations through the rasterized UV space, and naturally supports

3DMM-based editing, *e.g.*, avatar modeling by changing the shape and expression codes. We showcase this ability by directly swapping the shape and expression codes of given source identities onto the target instances by driving the learned Gaussians. As shown in Fig. 8, the reenactment results maintain their original texture details but accurately follow the shape and expression of the given source input. This application has the potential to facilitate avatar editing in game engines and media creation.

**Regional-based Editing.** In addition to global interpolation and transfer capabilities, GAUSSIAN3DIFF provides support for region-based editing, allowing modification exclusively within the semantic region defined by the UV mask. This functionality is illustrated in Fig. 9, where we showcase the transfer of corresponding source Gaussians (geometry) to the target, guided by the provided mask. The transferred results exhibit the same shape as the source within the defined semantic region, while the remaining areas remain unchanged. Benefiting from the UV space design, regional editing consistently produces semantically consistent results when transferring between mouth/nose regions of varying sizes across different identities. Furthermore, this demonstration underscores that GAUSSIAN3DIFF can surpass 3DMM constraints, enhancing controllability and exhibiting significant potential for avatar personalization within game engines [16].

## 4.4. Ablation Study

We ablate the design choice of adopting local tri-planes as the payload here. Please check the supplementary for more ablations on the utilization of a shared convolutional decoder for generating UV feature maps and the choice of $K$ value in Gaussian blending.

**Local Tri-plane.** In our early experiments, we opted for a pure feature vector as the local payload to represent the textures within a local region. However, we observed that the reconstruction performance consistently reached limitations, even when overfitting to a single instance. As visualized in Fig. 10, this motivated us to employ a tiny tri-plane as the texture payload. For both settings, we utilized 1024

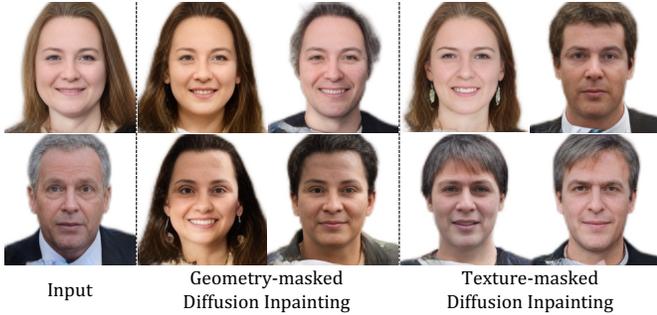Input | Geometry-masked Diffusion Inpainting | Texture-masked Diffusion Inpainting

Figure 7. **Diffusion-based Inpainting given Geometry or Texture Mask.** We provide either the geometry part (first 9 channels of the $256 \times 256 \times 33$ tensor $\mathcal{G}_0$) or the texture part (last 24 channels of the $256 \times 256 \times 33$ tensor $\mathcal{G}_0$) of the *upper face* as hints, and take the diffusion model $f_\theta$ in-paints the remaining details. As in columns $2-3$, all the generated results exhibit an identical upper-face shape, including the layout of the eyes and forehead, but with different textures. Conversely, the diffusion-inpainted results with texture masks (columns $4-5$) showcase an identical upper-face texture, encompassing features such as hair and forehead color, while varying in shape.



Figure 8. **3DMM-based Editing**. We reenact 5 random sampled source inputs (row-1) onto the targets (row-2, 3) by driving the target Gaussians through the adjustment of the inner 3DMM mesh using the shape and expression codes from the source. The reenactment results preserve their original texture while adapting to the shape and expression of the source inputs.

Gaussians to represent a scene and trained two variations till convergence. The results indicate that using a pure feature vector as the payload results in blurry view synthesis with a PSNR 21db and noisy depths. Conversely, our local tri-plane payload variations exhibit improved fidelity with PSNR 32db and cleaner surface reconstruction.

## 5. Conclusion, Limitation and Future Work

We have introduced GAUSSIAN3DIFF, a new 3D generative framework, and demonstrated its promising results across various scenarios. We first introduced a novel representation based on 3DMM anchored 3D Gaussians with tri-
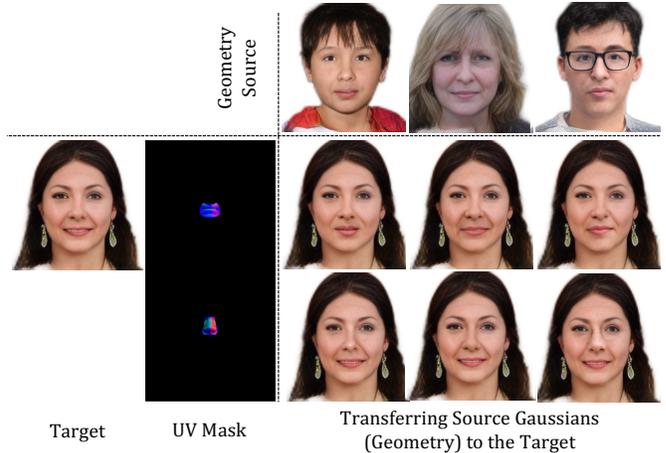


Figure 9. **Regional Editing with UV Mask**. The UV-space design in GAUSSIAN3DIFF enables the editing of specific semantic regions defined on the UV map. Given diffusion-sampled instances, we transfer the geometry shapes of the "nose" and "mouth" from the source identities to the target while leaving the remaining areas unchanged.
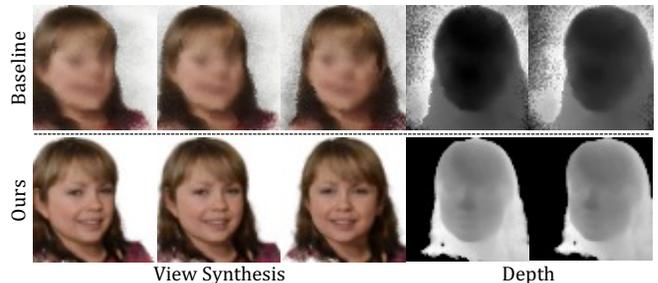


Figure 10. **Ablation Study on Local Tri-plane.** Using raw feature vectors as the payload lacks the ability to encode spatial information, and our local tri-plane design holds larger capacity and better reconstruction results.

plane payloads, which allows us to decouple the underlying smooth geometry and deformation from the complex volumetric appearance. Importantly, our representation can be stored in the UV space that is amenable to generative modelling. We then proposed a method to simultaneously reconstruct and learn a latent space for our 3D representations via multi-view supervision, upon which we train a 2D diffusion model to perform various editing tasks. We validate our framework on the synthetic dataset based on Panohead [1], which contains diverse, 360-degree view of photo-realistic human heads, though it has very limited variance in expressions. For future work, a natural follow up will be to extended our method to full body and introduce text/segmentation control [71] on 3D Gaussians. Moreover, adapting our framework on 3D datasets like ShapeNet [11] and Objaverse [12] is also meaningful. Besides, efficient high-res rendering and the support of splatting [31] is also under-explored.

# References

[1] Sizhe An, Hongyi Xu, Yichun Shi, Guoxian Song, Umit Y. Ogras, and Linjie Luo. Panohead: Geometry-aware 3d full-head synthesis in 360deg. In *CVPR*, pages 20950–20959, 2023. 1, 2, 4, 5, 6, 8

[2] Titas Anciukevičius, Zexiang Xu, Matthew Fisher, Paul Henderson, Hakan Bilen, Niloy J Mitra, and Paul Guerrero. Renderdiffusion: Image diffusion for 3d reconstruction, inpainting and generation. In *CVPR*, pages 12608–12618, 2023. 2

[3] Ziqian Bai, Feitong Tan, Zeng Huang, Kripasindhu Sarkar, Danhang Tang, Di Qiu, Abhimitra Meka, Ruofei Du, Mingsong Dou, Sergio Orts-Escolano, et al. Learning personalized high quality volumetric head avatars from monocular rgb videos. In *CVPR*, pages 16890–16900, 2023. 3

[4] Victor Besnier, Himalaya Jain, Andrei Bursuc, Matthieu Cord, and Patrick P'erez. This Dataset Does Not Exist: Training Models from Generated Images. *ICASSP*, 2020. 2

[5] Piotr Bojanowski, Armand Joulin, David Lopez-Paz, and Arthur Szlam. Optimizing the latent space of generative networks. *ICLR*, 2018. 4

[6] Andrew Brock, Jeff Donahue, and Karen Simonyan. Large scale GAN training for high fidelity natural image synthesis. In *ICLR*. OpenReview.net, 2019. 2

[7] Rohan Chabra, Jan Eric Lenssen, Eddy Ilg, Tanner Schmidt, Julian Straub, Steven Lovegrove, and Richard Newcombe. Deep local shapes: Learning local SDF priors for detailed 3D reconstruction. In *ECCV*, 2020. 3

[8] Eric Chan, Marco Monteiro, Petr Kellnhofer, Jiajun Wu, and G. Wetzstein. Pi-GAN: Periodic Implicit Generative Adversarial Networks for 3D-Aware Image Synthesis. In *CVPR*, 2021. 1, 2

[9] Eric R. Chan, Connor Z. Lin, Matthew A. Chan, Koki Nagano, Boxiao Pan, Shalini De Mello, Orazio Gallo, Leonidas Guibas, Jonathan Tremblay, Sameh Khamis, Tero Karras, and Gordon Wetzstein. Efficient geometry-aware 3D generative adversarial networks. In *CVPR*, 2022. 1, 2, 5

[10] Eric R. Chan, Koki Nagano, Matthew A. Chan, Alexander W. Bergman, Jeong Joon Park, Axel Levy, Miika Aittala, Shalini De Mello, Tero Karras, and Gordon Wetzstein. GeNVS: Generative novel view synthesis with 3D-aware diffusion models. In *arXiv*, 2023. 2

[11] Angel X. Chang, Thomas Funkhouser, Leonidas Guibas, Pat Hanrahan, Qixing Huang, Zimo Li, Silvio Savarese, Manolis Savva, Shuran Song, Hao Su, Jianxiong Xiao, Li Yi, and Fisher Yu. ShapeNet: An Information-Rich 3D Model Repository. Technical Report arXiv:1512.03012 [cs.GR], Stanford University — Princeton University — Toyota Technological Institute at Chicago, 2015. 8

[12] Matt Deitke, Dustin Schwenk, Jordi Salvador, Luca Weihs, Oscar Michel, Eli VanderBilt, Ludwig Schmidt, Kiana Ehsani, Aniruddha Kembhavi, and Ali Farhadi. Objaverse: A universe of annotated 3d objects. *arXiv preprint arXiv:2212.08051*, 2022. 8

[13] Jiankang Deng, Jia Guo, Niannan Xue, and Stefanos Zafeiriou. ArcFace: Additive angular margin loss for deep face recognition. In *CVPR*, 2019. 5

[14] Prafulla Dhariwal and Alexander Nichol. Diffusion models beat gans on image synthesis. *NIPS*, 34:8780–8794, 2021. 1, 2

[15] Emilien Dupont, Hyunjik Kim, SM Eslami, Danilo Rezende, and Dan Rosenbaum. From data to functa: Your data point is a function and you can treat it like one. *arXiv preprint arXiv:2201.12204*, 2022. 2

[16] Unreal Engine. MetaHuman - Realistic Person Creator. 7

[17] Guy Gafni, Justus Thies, Michael Zollhöfer, and Matthias Nießner. Dynamic neural radiance fields for monocular 4d facial avatar reconstruction. In *CVPR*, pages 8649–8658, 2021. 3

[18] Guy Gafni, Justus Thies, Michael Zollhöfer, and Matthias Nießner. Dynamic neural radiance fields for monocular 4d facial avatar reconstruction. In *CVPR*, 2021. 5

[19] Ian J. Goodfellow, Jean Pouget-Abadie, Mehdi Mirza, Bing Xu, David Warde-Farley, Sherjil Ozair, Aaron C. Courville, and Yoshua Bengio. Generative adversarial nets. In *NIPS*, 2014. 2

[20] Philip-William Grassal, Malte Prinzler, Titus Leistner, Carsten Rother, Matthias Nießner, and Justus Thies. Neural head avatars from monocular rgb videos. In *CVPR*, pages 18653–18664, 2022. 3

[21] Jiatao Gu, Lingjie Liu, Peng Wang, and Christian Theobalt. StyleNeRF: A style-based 3D-aware generator for high-resolution image synthesis. In *ICLR*, 2021. 1, 2

[22] Jiatao Gu, Qingzhe Gao, Shuangfei Zhai, Baoquan Chen, Lingjie Liu, and Josh Susskind. Learning controllable 3d diffusion models from single-view images. *arXiv preprint arXiv:2304.06700*, 2023. 2, 5

[23] Philipp Henzler, Niloy J Mitra, and Tobias Ritschel. Escaping plato's cave: 3D shape from adversarial rendering. In *ICCV*, 2019. 2

[24] Jonathan Ho, Ajay Jain, and Pieter Abbeel. Denoising diffusion probabilistic models. In *NIPS*, pages 6840–6851. Curran Associates, Inc., 2020. 1, 2

[25] Fangzhou Hong, Zhaoxi Chen, Yushi Lan, Liang Pan, and Ziwei Liu. EVA3D: Compositional 3d human generation from 2d image collections. In *ICLR*, 2022. 2

[26] Ali Jahanian, Lucy Chai, and Phillip Isola. On the" steerability" of generative adversarial networks. *ICLR*, 2020. 2

[27] Ali Jahanian, Xavier Puig, Yonglong Tian, and Phillip Isola. Generative models as a data source for multiview representation learning. *ICLR*, 2022. 2

[28] Ajay Jain, Ben Mildenhall, Jonathan T. Barron, Pieter Abbeel, and Ben Poole. Zero-shot text-guided object generation with dream fields. In *CVPR*, 2022. 2

[29] Tero Karras, Samuli Laine, and Timo Aila. A style-based generator architecture for generative adversarial networks. In *CVPR*, 2019. 2, 5

[30] Tero Karras, Samuli Laine, Miika Aittala, Janne Hellsten, Jaakko Lehtinen, and Timo Aila. Analyzing and improving the image quality of StyleGAN. In *CVPR*, 2020. 2

[31] Bernhard Kerbl, Georgios Kopanas, Thomas Leimkühler, and George Drettakis. 3d gaussian splatting for real-time radiance field rendering. *ACM Transactions on Graphics (ToG)*, 42(4):1–14, 2023. 3, 8

[32] Leonid Keselman and Martial Hebert. Approximate differentiable rendering with algebraic surfaces. In *European Conference on Computer Vision*, pages 596–614. Springer, 2022. 3

[33] Yushi Lan, Chen Change Loy, and Bo Dai. DDF: Correspondence distillation from nerf-based gan. *IJCV*, 2022. 2, 4, 5

[34] Yushi Lan, Xuyi Meng, Shuai Yang, Chen Change Loy, and Bo Dai. E3dge: Self-supervised geometry-aware encoder for style-based 3d gan inversion. In *CVPR*, 2023. 2, 4

[35] Tianye Li, Timo Bolkart, Michael. J. Black, Hao Li, and Javier Romero. Learning a model of facial shape and expression from 4D scans. *TOG*, 36(6), 2017. 3, 5

[36] Stephen Lombardi, Tomas Simon, Gabriel Schwartz, Michael Zollhoefer, Yaser Sheikh, and Jason Saragih. Mixture of volumetric primitives for efficient neural rendering. *ACM Trans. Graph.*, 40(4), 2021. 3

[37] Stephen Lombardi, Tomas Simon, Gabriel Schwartz, Michael Zollhoefer, Yaser Sheikh, and Jason Saragih. Mixture of volumetric primitives for efficient neural rendering. *ACM Transactions on Graphics (TOG)*, 40(4):1–13, 2021. 3

[38] Matthew Loper, Naureen Mahmood, Javier Romero, Gerard Pons-Moll, and Michael J Black. Smpl: A skinned multi-person linear model. *TOG*, 34(6):1–16, 2015. 3

[39] Lars Mescheder, Michael Oechsle, Michael Niemeyer, Sebastian Nowozin, and Andreas Geiger. Occupancy networks: Learning 3D reconstruction in function space. In *CVPR*, 2019. 2

[40] Ben Mildenhall, Pratul P Srinivasan, Matthew Tancik, Jonathan T Barron, Ravi Ramamoorthi, and Ren Ng. NeRF: Representing scenes as neural radiance fields for view synthesis. In *ECCV*. Springer, 2020. 2, 3

[41] Norman Müller, Yawar Siddiqui, Lorenzo Porzi, Samuel Rota Bulo, Peter Kontschieder, and Matthias Nießner. Diffrf: Rendering-guided 3d radiance field diffusion. In *CVPR*, pages 4328–4338, 2023. 2

[42] Thu Nguyen-Phuoc, Chuan Li, Lucas Theis, Christian Richardt, and Yongliang Yang. HoloGAN: Unsupervised Learning of 3D Representations From Natural Images. In *ICCV*, 2019. 2

[43] Michael Niemeyer and Andreas Geiger. Giraffe: Representing scenes as compositional generative neural feature fields. In *CVPR*, pages 11453–11464, 2021. 2

[44] Roy Or-El, Xuan Luo, Mengyi Shan, Eli Shechtman, Jeong Joon Park, and Ira Kemelmacher-Shlizerman. StyleSDF: High-Resolution 3D-Consistent Image and Geometry Generation. In *CVPR*, 2021. 2

[45] Xingang Pan, Bo Dai, Ziwei Liu, Chen Change Loy, and Ping Luo. Do 2D GANs know 3D shape? Unsupervised 3D Shape Reconstruction from 2D Image GANs. In *ICLR*, 2021. 2

[46] Xingang Pan, Xiaohang Zhan, Bo Dai, Dahua Lin, Chen Change Loy, and Ping Luo. Exploiting Deep Generative Prior for Versatile Image Restoration and Manipulation. *PAMI*, 44:7474–7489, 2022. 2

[47] Jeong Joon Park, Peter Florence, Julian Straub, Richard Newcombe, and Steven Lovegrove. Deepsdf: Learning continuous signed distance functions for shape representation. In *CVPR*, 2019. 4

[48] Jeong Joon Park, Peter Florence, Julian Straub, Richard Newcombe, and Steven Lovegrove. Deepsdf: Learning continuous signed distance functions for shape representation. In *CVPR*, pages 165–174, 2019. 2

[49] Keunhong Park, Utkarsh Sinha, Jonathan T. Barron, Sofien Bouaziz, Dan B Goldman, Steven M. Seitz, and Ricardo Martin-Brualla. Nerfies: Deformable neural radiance fields. In *ICCV*, 2021. 3, 5

[50] Keunhong Park, Utkarsh Sinha, Peter Hedman, Jonathan T. Barron, Sofien Bouaziz, Dan B Goldman, Ricardo Martin-Brualla, and Steven M. Seitz. Hypernerf: A higher-dimensional representation for topologically varying neural radiance fields. *TOG*, 40(6), 2021. 5

[51] Georgios Pavlakos, Vasileios Choutas, Nima Ghorbani, Timo Bolkart, Ahmed A. A. Osman, Dimitrios Tzionas, and Michael J. Black. Expressive body capture: 3D hands, face, and body from a single image. In *CVPR*, pages 10975–10985, 2019. 3

[52] Ben Poole, Ajay Jain, Jonathan T. Barron, and Ben Mildenhall. Dreamfusion: Text-to-3d using 2d diffusion. *ICLR*, 2022. 2

[53] Alec Radford, Jong Wook Kim, Chris Hallacy, Aditya Ramesh, Gabriel Goh, Sandhini Agarwal, Girish Sastry, Amanda Askell, Pamela Mishkin, Jack Clark, Gretchen Krueger, and Ilya Sutskever. Learning transferable visual models from natural language supervision. In *ICML*, 2021. 5

[54] Daniel Rebain, Mark Matthews, Kwang Moo Yi, Dmitry Lagun, and Andrea Tagliasacchi. LOLNeRF: Learn from one look, 2022. 4

[55] Robin Rombach, Andreas Blattmann, Dominik Lorenz, Patrick Esser, and Björn Ommer. High-resolution image synthesis with latent diffusion models. In *CVPR*, pages 10684–10695, 2022. 2, 3, 5

[56] Olaf Ronneberger, Philipp Fischer, and Thomas Brox. U-net: Convolutional networks for biomedical image segmentation. In *MICCAI*, pages 234–241. Springer, 2015. 5

[57] Chitwan Saharia, William Chan, Saurabh Saxena, Lala Li, Jay Whang, Emily L Denton, Kamyar Ghasemipour, Raphael Gontijo Lopes, Burcu Karagol Ayan, Tim Salimans, et al. Photorealistic text-to-image diffusion models with deep language understanding. *NIPS*, 35:36479–36494, 2022. 2

[58] Chitwan Saharia, William Chan, Saurabh Saxena, Lala Li, Jay Whang, Emily L. Denton, Seyed Kamyar Seyed Ghasemipour, Burcu Karagol Ayan, Seyedeh Sara Mahdavi, Raphael Gontijo Lopes, Tim Salimans, Jonathan Ho, David J. Fleet, and Mohammad Norouzi. Photorealistic text-to-image diffusion models with deep language understanding. *NIPS*, 2022. 2, 5

[59] Katja Schwarz, Yiyi Liao, Michael Niemeyer, and Andreas Geiger. GRAF: Generative radiance fields for 3D-aware image synthesis. In *NIPS*, 2020. 1, 2

[60] Jessica Shue, Eric Chan, Ryan Po, Zachary Ankner, Jiajun Wu, and Gordon Wetzstein. 3d neural field generation using triplane diffusion. *CVPR*, pages 20875–20886, 2022. 1

[61] Yang Song, Jascha Sohl-Dickstein, Diederik P Kingma, Abhishek Kumar, Stefano Ermon, and Ben Poole. Score-based

generative modeling through stochastic differential equations. In *ICLR*, 2021. 1, 2, 5

[62] Jingxiang Sun, Xuan Wang, Yong Zhang, Xiaoyu Li, Qi Zhang, Yebin Liu, and Jue Wang. FENeRF: Face editing in neural radiance fields, 2021. 1, 2

[63] Jingxiang Sun, Xuan Wang, Yichun Shi, Lizhen Wang, Jue Wang, and Yebin Liu. Ide-3d: Interactive disentangled editing for high-resolution 3d-aware portrait synthesis. *ACM Transactions on Graphics (TOG)*, 41(6):1–10, 2022. 1, 2, 3, 5

[64] Jingxiang Sun, Xuan Wang, Lizhen Wang, Xiaoyu Li, Yong Zhang, Hongwen Zhang, and Yebin Liu. Next3d: Generative neural texture rasterization for 3d-aware head avatars. In *CVPR*, 2023. 1

[65] Feitong Tan, Sean Fanello, Abhimitra Meka, Sergio Orts-Escolano, Danhang Tang, Rohit Pandey, Jonathan Taylor, Ping Tan, and Yinda Zhang. Volux-gan: A generative model for 3d face synthesis with hdri relighting. In *ACM SIGGRAPH 2022 Conference Proceedings*, pages 1–9, 2022. 2

[66] Tengfei Wang, Bo Zhang, Ting Zhang, Shuyang Gu, Jianmin Bao, Tadas Baltrusaitis, Jingjing Shen, Dong Chen, Fang Wen, Qifeng Chen, et al. Rodin: A generative model for sculpting 3d digital avatars using diffusion. In *CVPR*, pages 4563–4573, 2023. 1, 3, 4, 6

[67] Xintao Wang, Ke Yu, Shixiang Wu, Jinjin Gu, Yihao Liu, Chao Dong, Yu Qiao, and Chen Change Loy. Esrgan: Enhanced super-resolution generative adversarial networks. In *ECCVW*, 2018. 5

[68] Shuai Yang, Liming Jiang, Ziwei Liu, , and Chen Change Loy. VToonify: Controllable high-resolution portrait video style transfer. *ACM Transactions on Graphics (TOG)*, 41(6): 1–15, 2022. 2

[69] Yi Yang and Deva Ramanan. Articulated human detection with flexible mixtures of parts. *PAMI*, 35:2878–2890, 2013. 5

[70] Xiaohui Zeng, Arash Vahdat, Francis Williams, Zan Gojcic, Or Litany, Sanja Fidler, and Karsten Kreis. Lion: Latent point diffusion models for 3d shape generation. In *NIPS*, 2022. 2

[71] Lvmin Zhang, Anyi Rao, and Maneesh Agrawala. Adding conditional control to text-to-image diffusion models. In *ICCV*, 2023. 8

[72] Richard Zhang, Phillip Isola, Alexei A Efros, Eli Shechtman, and Oliver Wang. The unreasonable effectiveness of deep features as a perceptual metric. In *CVPR*, 2018. 4

[73] Xiaoshuai Zhang, Sai Bi, Kalyan Sunkavalli, Hao Su, and Zexiang Xu. Nerfusion: Fusing radiance fields for large-scale scene reconstruction. In *CVPR*, pages 5449–5458, 2022. 3

[74] Xiaoshuai Zhang, Abhijit Kundu, Thomas Funkhouser, Leonidas Guibas, Hao Su, and Kyle Genova. Nerflets: Local radiance fields for efficient structure-aware 3d scene representation from 2d supervision. In *CVPR*, 2023. 3

[75] Yuxuan Zhang, Huan Ling, Jun Gao, Kangxue Yin, Jean-Francois Lafleche, Adela Barriuso, Antonio Torralba, and Sanja Fidler. DatasetGAN: Efficient labeled data factory with minimal human effort. In *CVPR*, 2021. 2, 4

[76] Yufeng Zheng, Victoria Fernández Abrevaya, Marcel C. Bühler, Xu Chen, Michael J. Black, and Otmar Hilliges. I M Avatar: Implicit morphable head avatars from videos. In *CVPR*, 2022. 3